

Quantitative study of buried heat sources by lock-in vibrothermography: an approach to crack characterization

This article has been downloaded from IOPscience. Please scroll down to see the full text article.

2009 J. Phys. D: Appl. Phys. 42 055502

(<http://iopscience.iop.org/0022-3727/42/5/055502>)

[The Table of Contents](#) and [more related content](#) is available

Download details:

IP Address: 158.227.68.58

The article was downloaded on 17/02/2009 at 08:28

Please note that [terms and conditions apply](#).

Quantitative study of buried heat sources by lock-in vibrothermography: an approach to crack characterization

A Mendioroz¹, E Apiñaniz¹, A Salazar¹, P Venegas² and I Sáez-Ocáriz²

¹ Departamento de Física Aplicada I, Escuela Técnica Superior de Ingeniería, Universidad del País Vasco, Alameda Urquijo s/n, 48013 Bilbao, Spain

² Centro de Tecnologías Aeronáuticas (CTA), Parque Tecnológico de Álava, Juan de la Cierva 1, 01510 Miñano, Spain

E-mail: arantza.mendioroz@ehu.es

Received 27 October 2008, in final form 25 November 2008

Published 17 February 2009

Online at stacks.iop.org/JPhysD/42/055502

Abstract

Vibrothermography has proven to be a useful technique for the detection of cracks, which reveal themselves as heat sources when mechanically excited in vibrothermography experiments. In this work we present a method to evaluate the size and depth of buried heat sources in metallic samples, from lock-in vibrothermography measurements. We have developed a theoretical model allowing us to calculate the surface temperature produced by modulated buried heat sources of arbitrary shape and power distribution by integrating the contribution of point-like heat sources over the entire heat source extension. In order to test the validity of the model, we have chosen homogeneous and rectangular heat sources, perpendicular to the sample surface. We have prepared calibrated heat sources by attaching two flat pieces of stainless steel and controlling the tightness with screws. Measurements of the surface temperature by an infrared video camera have been compared with the predictions of the theoretical model. The agreement between experimental and theoretical results confirms that lock-in vibrothermography is an efficient tool not only to detect but also to characterize the geometrical parameters of inner heat sources.

1. Introduction

Vibrothermography or thermo-sonics was introduced in the late 1970s as a new type of excitation in the field of thermographic nondestructive evaluation (NDE) for the detection of defects such as cracks or delaminations [1–3]. In contrast to the more classical thermography set-up in which the energy is delivered at the sample surface by optical means, in vibrothermographic arrangements the sample is mechanically excited by sonic or ultrasonic oscillations. The excitation is carried out by coupling an ultrasonic transducer to the sample surface. In general, the propagation of the damped acoustic waves along the material converts mechanical energy into thermal energy, but in the vicinity of the defects the energy dissipation is bigger due to friction between the faces of the defect and/or stress concentration in the surrounding area. In metals, where the acoustical damping is relatively low, this

mechanical excitation acts as a selective inner heat source, located at the defects, that diffuses inside the material and can be detected as a temperature variation at its surface by means of an infrared (IR) video camera.

As in optically excited IR thermography, two configurations have been mainly implemented in vibrothermography: one is the so-called lock-in vibrothermography [4] in which the high frequency oscillation is amplitude- (or frequency-) modulated at a low frequency and the detection lock-in system (synchronized with the amplitude varying input signal) detects the amplitude and phase of the surface temperature. The second configuration, called burst vibrothermography or sonic IR imaging [5], is based on the excitation of the sample by a brief (typically 50–200 ms) ultrasonic pulse and on the detection of the surface temperature as a function of time, also by an IR camera. In any of the preceding configurations, vibrothermography has proven to be a useful technique in the

rather difficult problem of detecting vertical cracks, and its utility has been tested in a wide variety of materials such as metals, polymers and composites [4–6]. In the case of photothermal techniques, the difficulty of detecting vertical cracks arises from the fact that when the optical energy is uniformly delivered at the sample surface the main heat flux is also perpendicular to the surface and thus the thermal waves are very slightly scattered by the defects. In consequence, the presence of these defects does not produce significant signatures in the sample surface temperature. In order to overcome this difficulty, more sophisticated photothermal and other types of thermographic techniques such as induction thermography [7], mirage effect [8] or stimulated differential IR radiometry [9] have been used to detect vertical cracks. More recently, other techniques have also been developed for the same purpose, such as forced diffusion thermal imaging [10], which uses a non-uniform moving pattern of IR radiation to heat the sample surface, and a flying-spot camera [11], where the laser beam and the detection system are jointly scanned over the sample surface at a constant speed and with different offsets. Some of the preceding methods are able to detect vertical cracks, but their sensitivity is poor [8, 9]. Regarding the two latter techniques, they have proven to be useful for the detection of both open and kissing cracks, reaching the sample surface and, in the case of a flying-spot camera, inner vertical cracks can also be detected [12].

On the other hand, the mechanical excitation in vibrothermography is especially suitable for the detection of kissing or closed cracks and open microcracks [13] since friction between the two sides of the crack turns the whole defect into a heat source and, besides, its use is not restricted to cracks reaching the sample surface. When the geometry of the crack and the physical properties of the medium are such that friction takes place only at certain positions, the heat sources generated with vibrothermography experiments do not extend over the whole crack [14], meaning that, properly speaking, vibrothermography experiments lead to ‘heat sources detection’, rather than ‘crack detection’. Accordingly, any attempt to characterize the crack using vibrothermography experiments should be understood, in general, as a characterization of heat sources. Actually, the attempts to characterize crack geometrical parameters using vibrothermography have been limited mainly to length estimations [14, 15], since at least the tips of the crack are always excited in vibrothermography experiments [14]. Nevertheless, for closed cracks, the entire defect turns into a heat source in vibrothermography experiments, giving the possibility of ‘defect characterization’.

Whatever configuration (modulated or pulsed) is used, the physical processes contributing to the measured temperature variations at the sample surface after the initial mechanical excitation are rather complex. These processes have been the subject of several studies, especially in the case of burst vibrothermography: the propagation of the acoustic wave inside the material [16–19], the mechanisms by which heat is generated at the defects [17–20] and the diffusion of this thermal energy to the sample surface [15]. Moreover, since the excitation method requires contact between the sample

and the vibration generator, experimental issues related to the particular configuration of piezoelectric transducer coupling, especially the way the sample is held in place, introduce even more complexity to the task of understanding the whole process [6].

In this work we focus on the study of the last step of this complex process, i.e. the diffusion of the thermal energy generated by a heat source excited at a crack in a lock-in vibrothermography experiment and the resulting surface temperature distribution. The contribution of our work is aimed at demonstrating the ability of lock-in vibrothermography to characterize the location and geometrical parameters of buried heat sources. In the case of closed cracks or microcracks, this would open the possibility of characterizing the defect itself, while for partially open cracks, only certain points of the crack would be located, especially the ends of the crack.

We have developed a theoretical model allowing us to calculate the surface temperature distribution produced by buried heat sources of an arbitrary shape and power distribution. The predictions of this general model have been tested in the particular case of homogeneous and rectangular heat sources perpendicular to the sample surface. The reasons for this choice are (1) that in order to test the validity of the model, calibrated samples of these characteristics are easy to construct and (2) that vertical cracks, which would lead to plane heat sources perpendicular to the surface, are difficult to detect. In our model, buried heat sources are formed by the superposition of infinitesimal point-like modulated sources. In this way, the surface temperature of the material is calculated by integrating the contribution of each point-like source over the entire source size. We have performed lock-in vibrothermography measurements on samples with calibrated vertical heat sources, which have been prepared by attaching two flat pieces of stainless steel and controlling the tightness with screws. The agreement between theoretical and experimental data confirms that lock-in vibrothermography is an efficient tool to determine the size and position of vertical and buried heat sources. This opens the possibility not only of detecting vertical cracks but also of estimating their geometrical parameters.

2. Theory and numerical calculations

We have modelled the resulting heat source generated at a vertical crack in a vibrothermography experiment as a flat and rectangular source of width b and height c , located at a depth d , beneath the surface of the sample of thickness e . For the sake of simplicity, the heat source is considered homogeneous. The geometry we have worked with is shown in figure 1, where the heat source is drawn in black. In lock-in vibrothermography the crack acts as a heat source modulated at the same frequency f ($\omega = 2\pi f$) as the amplitude of the ultrasonic source is modulated. In order to calculate the oscillation of the sample temperature produced by the rectangular modulated heat source, we decompose it as the superposition of infinitesimal modulated heat sources. If we consider a point-like heat source

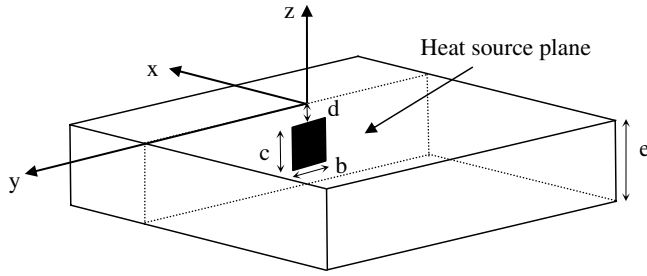


Figure 1. Geometry of the vertical heat source.

modulated at frequency f and located at coordinates $(0, y_0, z_0)$ in a homogeneous and infinite medium, the amplitude of the temperature oscillation at any point (x, y, z) of the material is given by [21]

$$T(x, y, z) = T_0 \frac{e^{-q\sqrt{x^2+(y-y_0)^2+(z-z_0)^2}}}{\sqrt{x^2+(y-y_0)^2+(z-z_0)^2}}, \quad (1)$$

where T_0 is a factor that depends on the strength of the heat source and on the thermal properties of the medium and $q = \sqrt{i\omega/D}$ is the thermal wave vector, with D the thermal diffusivity. Equation (1) represents a highly damped spherical thermal wave generated at $(0, y_0, z_0)$. The amplitude of the temperature oscillation corresponding to the entire rectangular heat source is obtained by integrating equation (1) over its whole size:

$$T(x, y, z) = \int_{-b/2}^{b/2} \int_{-(c+d)}^{-d} T_0 \frac{e^{-q\sqrt{x^2+(y-y_0)^2+(z-z_0)^2}}}{\sqrt{x^2+(y-y_0)^2+(z-z_0)^2}} dy_0 dz_0. \quad (2)$$

From equation (2) it is easy to calculate the sample temperature in the particular case of an infinitely large heat source ($b \rightarrow \infty$, $c \rightarrow \infty$ and $d \rightarrow 0$):

$$T(x) = \int_{-\infty}^{\infty} \int_{-\infty}^{\infty} T_0 \frac{e^{-q\sqrt{x^2+(y-y_0)^2+(z-z_0)^2}}}{\sqrt{x^2+(y-y_0)^2+(z-z_0)^2}} dy_0 dz_0 = 2\pi T_0 \frac{e^{-qx}}{q}, \quad (3)$$

which represents a damped plane thermal wave propagating along both directions of the x -axis.

Up to now we have not taken into account the influence of the front ($z = 0$) and rear ($z = -e$) sample surfaces in the heat propagation. If we consider adiabatic conditions, i.e. no heat transfer from the sample boundaries to the surroundings, the effect of both surfaces can be accounted for via the introduction of the images of the rectangle reflected at the front and rear surfaces, the so-called ‘image method’ [22]. In this way, the amplitude of the temperature oscillation at any point of the

sample is given by

$$T(x, y, z) = \int_{-b/2}^{b/2} \int_{-(c+d)}^{-d} T_0 \frac{e^{-q\sqrt{x^2+(y-y_0)^2+(z-z_0)^2}}}{\sqrt{x^2+(y-y_0)^2+(z-z_0)^2}} dy_0 dz_0 + \int_{-b/2}^{b/2} \int_d^{c+d} T_0 \frac{e^{-q\sqrt{x^2+(y-y_0)^2+(z-z_0)^2}}}{\sqrt{x^2+(y-y_0)^2+(z-z_0)^2}} dy_0 dz_0 + \int_{-b/2}^{b/2} \int_{-2e+d}^{-2e+c+d} T_0 \frac{e^{-q\sqrt{x^2+(y-y_0)^2+(z-z_0)^2}}}{\sqrt{x^2+(y-y_0)^2+(z-z_0)^2}} dy_0 dz_0 + \int_{-b/2}^{b/2} \int_{2e-c-d}^{2e-d} T_0 \frac{e^{-q\sqrt{x^2+(y-y_0)^2+(z-z_0)^2}}}{\sqrt{x^2+(y-y_0)^2+(z-z_0)^2}} dy_0 dz_0 + \dots, \quad (4)$$

where the first term is the contribution to the sample temperature due to the real heat source, the second term is the contribution due to the image of the heat source reflected at the front surface, the third term is the contribution due to the image of the heat source reflected at the rear surface, the fourth term is the contribution due to the image of the heat source after being reflected twice, first at the front surface and then at the rear surface, and so forth.

Although equation (4) allows us to calculate the whole temperature distribution of the sample, we are interested in calculating the temperature just at the sample surface ($z = 0$), where experimental data using IR thermography can be obtained. According to the symmetry of the images, the surface temperature reduces to

$$T(x, y) = 2 \int_{-b/2}^{b/2} \int_{-(c+d)}^{-d} T_0 \frac{e^{-q\sqrt{x^2+(y-y_0)^2+z_0^2}}}{\sqrt{x^2+(y-y_0)^2+z_0^2}} dy_0 dz_0 + 2 \int_{-b/2}^{b/2} \int_{-2e+d}^{-2e+c+d} T_0 \frac{e^{-q\sqrt{x^2+(y-y_0)^2+z_0^2}}}{\sqrt{x^2+(y-y_0)^2+z_0^2}} dy_0 dz_0 + 2 \int_{-b/2}^{b/2} \int_{-(2e+c+d)}^{-(2e+d)} T_0 \frac{e^{-q\sqrt{x^2+(y-y_0)^2+z_0^2}}}{\sqrt{x^2+(y-y_0)^2+z_0^2}} dy_0 dz_0 + \dots. \quad (5)$$

It is worth noting that even if the material is a metal, adiabatic boundary conditions might not be completely fulfilled at very low frequencies due to heat losses, so we have limited our calculations to frequencies above 0.1 Hz. We have performed numerical calculations of the surface temperature for AISI 304 stainless steel ($K = 10 \text{ W m}^{-1} \text{ K}^{-1}$ and $D = 4 \text{ mm}^2 \text{ s}^{-1}$) plates 1 cm thick using equation (5), for different sizes and depths of the heat source. The number of terms (images) in equation (5) that are needed to guarantee the convergence depends on the ratio between the thermal diffusion length ($\mu = \sqrt{D/\pi f}$) and the thickness of the sample e . In our calculations this ratio is always smaller than 0.5 and therefore only two pairs of images at each side of the sample are enough for the calculations to converge.

In order to illustrate the effect of the heat source width, b , on the surface temperature we have calculated profiles of the normalized amplitude and phase of the surface temperature

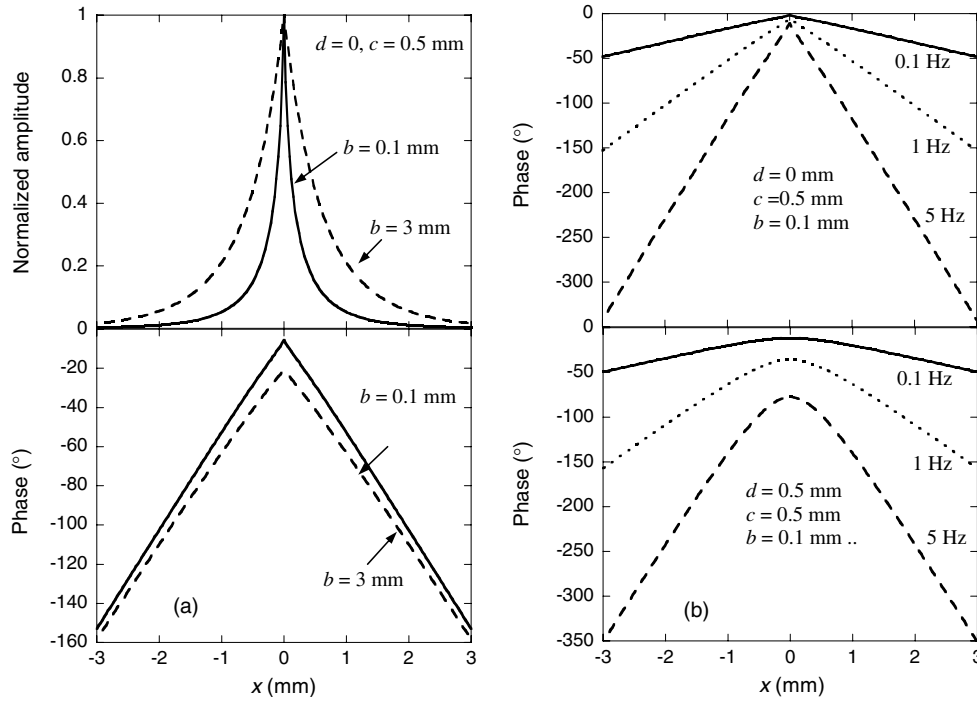


Figure 2. (a) Calculated amplitude and phase profiles along the x -axis of the surface temperature for two heat sources of height $c = 0.5$ mm, reaching the sample surface ($d = 0$) and having different widths $b = 0.1$ mm (solid line) and $b = 3$ mm (dashed line). A modulation frequency of 1 Hz has been used for the calculations. (b) Calculated phase profiles corresponding to two heat sources of the same dimensions ($b = 0.1$ mm and $c = 0.5$ mm) but different depths $d = 0$ mm (top) and $d = 0.5$ mm (bottom). These profiles have been calculated for three modulation frequencies.

along the x -axis for a heat source of height $c = 0.5$ mm reaching the surface ($d = 0$), at a modulation frequency of 1 Hz. Two different widths have been used: $b = 0.1$ mm (solid line) and $b = 3$ mm (dashed line). The results are shown in figure 2(a). As can be observed, the wider the heat source, the wider the amplitude profile along the x -axis is. In fact, as the width of the heat source increases the shape of the generated thermal wave changes from spherical to plane, whose amplitude decreases slowly due to the lack of the factor $1/r$ associated with the spherical wave. However, the phase profiles do not differ as much as the amplitudes do, since the factor $1/r$ does not affect the phase of the thermal wave.

Similarly, the effect of the heat source depth, d , on the temperature phase profiles along the x -axis is shown in figure 2(b) for two cracks having the same dimensions ($b = 0.1$ mm and $c = 0.5$ mm). On top, the source reaches the sample surface, while at the bottom, it is buried at a depth $d = 0.5$ mm. Profiles have been calculated for several modulation frequencies: 0.1, 1 and 5 Hz. Two interesting features can be observed in figure 2(b). (1) The profiles corresponding to the shallower source are sharper than those of the one buried beneath the surface, which look smoother. (2) Even more interesting is the fact that the maximum variation of the phase peak ranges from 0° to 45° for the heat source reaching the surface, while for the deeper one, the variation of the peak of the phase is much more pronounced with frequency.

Following this result, in figure 3 we have plotted the maximum values of both amplitude and phase versus the modulation frequency for cracks at two different depths ($d = 0$ mm in figure 3(a) and $d = 0.3$ mm in figure 3(b)) and

having different widths, but the same height ($c = 0.5$ mm). Regarding the behaviour of the peak amplitude, it can be observed that the deeper the source, the faster the temperature peak decreases with the modulation frequency, since the heat diffusion length decreases with the increase in frequency. As mentioned in the previous paragraph, the variation of the phase peak with frequency is much more pronounced for the deeper source than for the shallower one. On the other hand, for both depths the behaviour of the amplitude and phase peaks is sensitive to the width of the source, the phase being more sensitive than the amplitude in both cases. It is worth adding that the possibility of distinguishing between different source widths is better for a shallow source, as we are dealing with highly damped thermal waves. Although the results shown in figure 3 look promising regarding the possibility of identifying the geometrical parameters of the heat source, the method implies the evaluation of the amplitude and/or phase of a single pixel in the experimental surface temperature maps which, in practice, leads to significant errors. For this reason, in order to determine the geometrical parameters of the heat source, we decided to compare the whole experimental and theoretical phase profiles along the x -axis, together with additional profiles parallel to the x -axis and located at several distances from the origin. In the next section, we will compare the experimental results of the surface temperature phase with the simulations obtained by applying this model for the parameters corresponding to the experimental conditions.

As mentioned in the introduction, calculations provided by equation (5) can be easily improved for different geometries of the heat source, including non-flat shapes and inhomogeneous

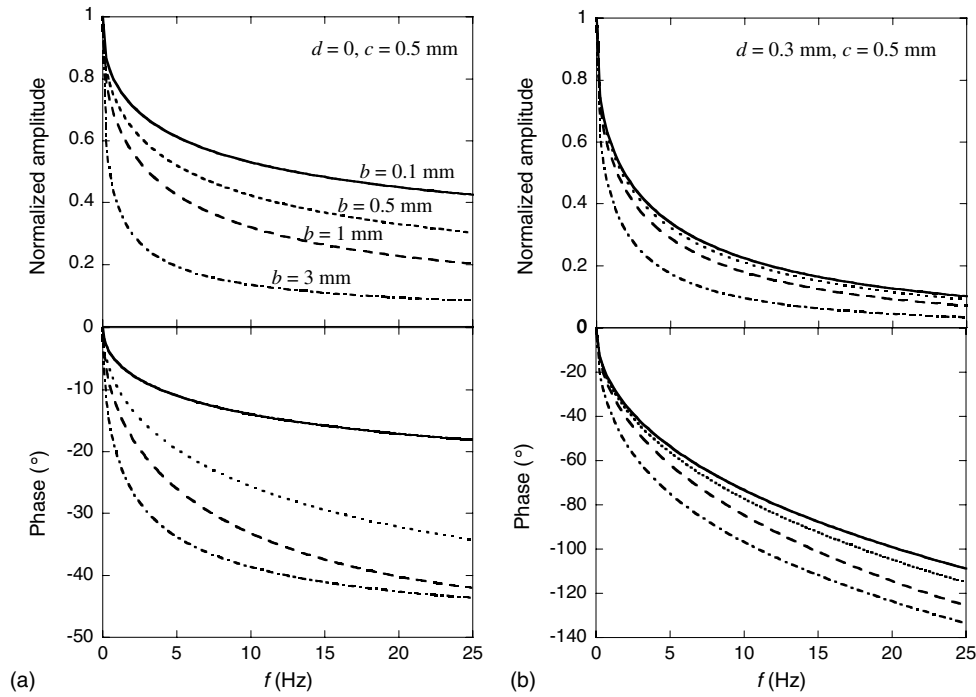


Figure 3. Frequency dependence of the maximum values of the temperature amplitude and phase for heat sources of the same height $c = 0.5$ mm and two different depths: (a) $d = 0$ mm, (b) $d = 0.3$ mm. The calculations have been performed for different source widths: $b = 0.1$ mm (solid line), $b = 0.5$ mm (dotted line), $b = 1$ mm (dashed line) and $b = 3$ mm (dotted–dashed line).

heat sources, by just appropriately selecting the power distribution and integration limits.

3. Experimental results and discussion

As mentioned in the introduction, in vibrothermography experiments a crack reveals itself as a heat source inside the material. We intend to test the ability of our theoretical model to determine the size and position of flat heat sources, perpendicular to the surface, from vibrothermography experiments, so we need to build samples with well-localized inner heat sources. For that purpose, we have prepared samples simulating the presence of a heat source by attaching two pieces of AISI 304 stainless steel against each other through a flat surface of dimensions 1 cm \times 1 cm. In order to better localize the heat sources in an easy way, we have introduced between these two pieces a rectangular thin sheet of copper, whose dimensions are at least one order of magnitude smaller than those of the flat surface. The friction between this copper sheet and the stainless steel pieces will be our heat source in vibrothermography experiments. In order to guarantee that mechanical contact only takes place at the location of the copper sheet, we also use two additional copper plates, far enough from the measuring surface to prevent heat produced at these positions to reach the surface where data will be taken, even at the lowest modulation frequency. The size and depth of the copper sheet can be modified in order to perform measurements for different geometrical parameters of the heat source. The two stainless steel pieces are held together by means of two screws, allowing us to modify the pressure between them. Figure 4(a) shows a diagram of the fabricated samples. In figures 4(b) and (c) we show the details of the size

and location of the copper sheet acting as a heat source in the two samples we have measured. The two protecting copper plates are also drawn at the bottom. In figure 4(d) the whole sample as prepared for a measurement is shown. Finally, as an example, figure 4(e) shows a phase thermogram recorded at a modulation frequency of 1.0 Hz.

The measurements were performed using commercial lock-in vibrothermography equipment (UTvis from EDEVIS). The surface temperature data were collected with an IR camera (Silver 480M from CEDIP), synchronized with the amplitude varying input signal. For the measurements the sample was placed between a teflon block and the horn tip, which applies a preload pressure of 3 bar. We used an aluminium sheet to improve the mechanical contact between the tip and the sample. The equipment we have used to carry out the experiments is able to generate ultrasound frequencies ranging from 15 to 25 kHz. It has recently been demonstrated [23] that for specimens whose size is of the order of the ultrasound wavelength, normal modes of the specimen can be excited in lock-in vibrothermography experiments. If a part of the crack is located at the position of a node of the standing wave the result is the absence of vibration of the two sides of the crack, and as a consequence, the crack cannot be detected. This is the reason why performing frequency sweeps is useful in order to determine the most suitable ultrasound frequency to detect the crack in a particular specimen. We have performed such sweeps in our samples and have found an optimum ultrasound frequency of 19.75 kHz, at which data have been taken.

We performed measurements for different pressures between the two faces of the steel pieces by changing the tightness of the screws. At both ends, for very tight and very loose screws, the signal was very poor, indicating that

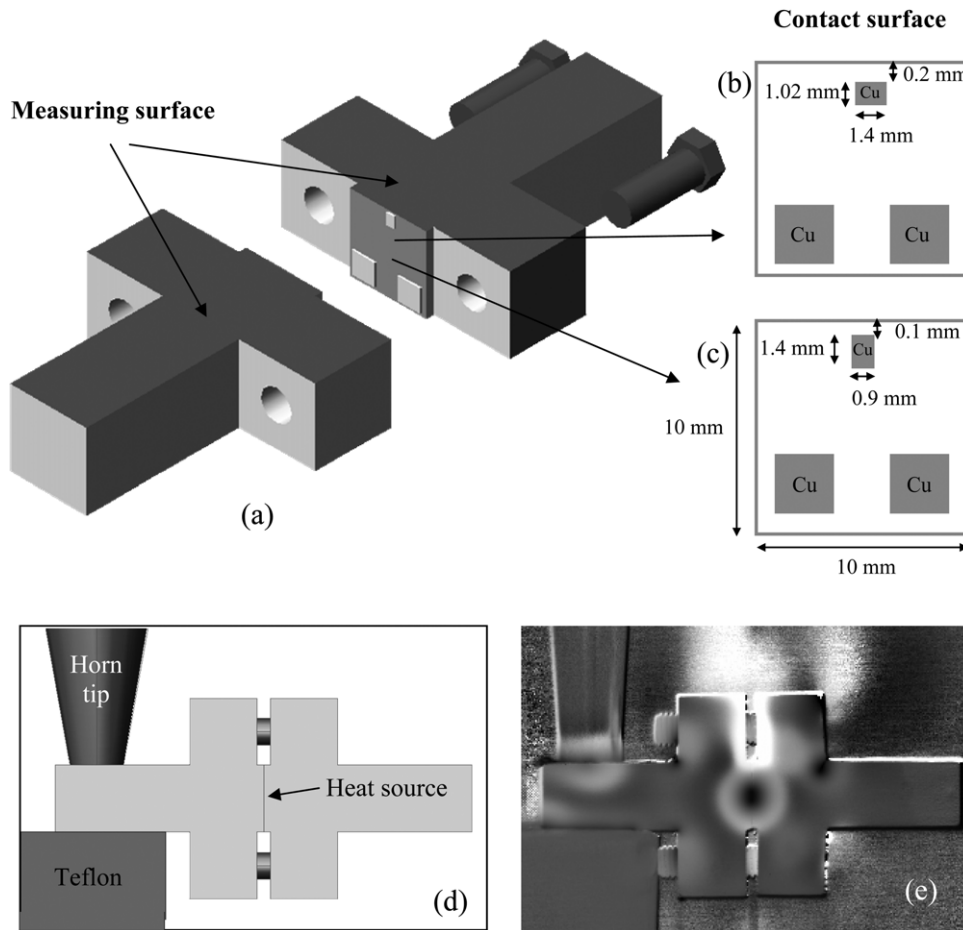


Figure 4. (a) Diagram of the fabricated sample used for the vibrothermography measurements. (b) and (c) Diagrams showing the contact surface simulating the two heat sources that we have measured. The small copper sheet acts as a heat source while the two protecting sheets are placed at the bottom. (d) Side view of the surface where measurements have been performed, with the two pieces attached and held in place, in contact with the tip, as prepared for a measurement. (e) Experimental surface temperature phase map corresponding to a modulation frequency of 1.0 Hz.

when the pressure between the two faces of the ‘defect’ is high and when the faces are not in contact no heat is generated and, as a consequence, it becomes barely detectable. The same conclusion has been reached in studies of the crack closure effect on its detectability in sonic IR imaging [24]. Following these results, we performed the measurements at an intermediate pressure between the two faces of the steel piece.

We have performed vibrothermography measurements for the configurations depicted in figures 4(b) and (c). In figure 5(a) we show the experimental surface temperature phase map corresponding to the experimental conditions shown in figure 4(b), in which the heat source has a width $b = 1.4$ mm, a height $c = 1.02$ mm and is located at a depth $d = 0.2$ mm. The data correspond to a modulation frequency of 1 Hz. It is worth mentioning that the lock-in process adds an arbitrary phase shift to the experimental phase. We have calculated the corresponding shifted surface phase map for these geometrical parameters using equation (5); it is shown in figure 5(b). As can be seen, the experimental and calculated phase maps look very similar. In order to quantitatively compare both maps, we have plotted the phase versus the distance for the three profiles 1, 2 and 3, depicted in figures 5(a) and (b), corresponding to the centre of the

crack, and 0.8 and 1.6 mm away from the centre, respectively. The result is shown in figure 5(c). As can be observed, the agreement between the experimental (symbols) and calculated profiles (solid lines) at different positions along the heat source length is very good. In order to investigate the capabilities of the technique to distinguish between different geometries, we have performed measurements for different positions and sizes of the copper sheet. As an example, in figure 6 we show the data corresponding to the geometry shown in figure 4(c) (width $b = 0.9$ mm, height $c = 1.4$ mm and depth $d = 0.1$ mm) at the same modulation frequency of 1 Hz, using the same procedure as in the previous case.

The comparison of figures 5 and 6 deserves some comments: (1) the shape of the maps follows the geometry of the heat sources, the longer one being that corresponding to the longest copper sheet along the measuring surface. (2) The agreement between the theoretical and experimental profiles is very good in both cases. Concerning the experimental evolution of the phase profile as the distance to the centre of the heat source is increased, it is faster for the narrowest copper sheet (figure 5) than for the longest one, as predicted by the theory.

For both samples, data were taken at several modulation frequencies ranging from 0.1 to 10 Hz. The agreement between

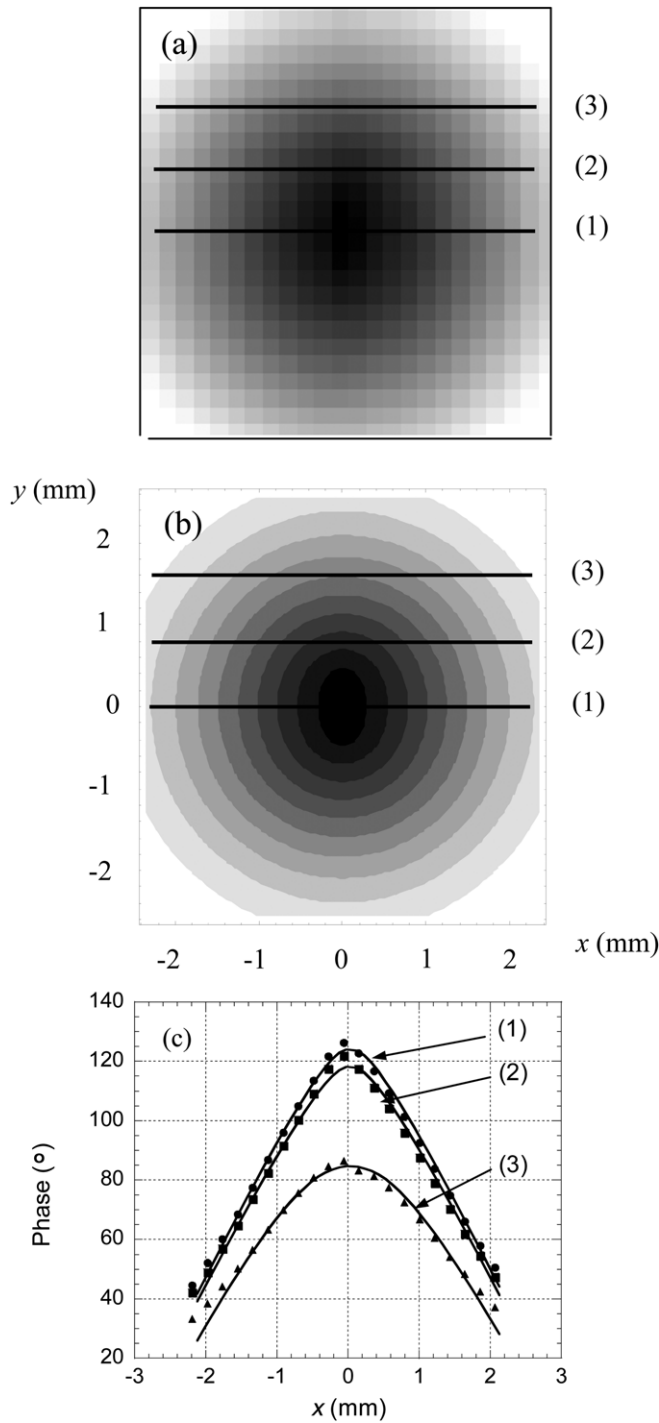


Figure 5. Experimental (a) and calculated (b) surface phase temperature maps for the heat source shown in figure 4(b). The grey scale is not comparable in both images. (c) Experimental (symbols) and calculated (solid lines) phase profiles along the lines depicted in the upper figures.

the experimental and theoretical results is good up to 5 Hz but becomes poorer at higher frequencies. This could be related to the lack of spatial resolution of the experimental equipment for high modulation frequencies together with the low signal-to-noise ratio, which diminishes as f increases.

These results show that the simple theory we have developed is able to reproduce the experimental data quite

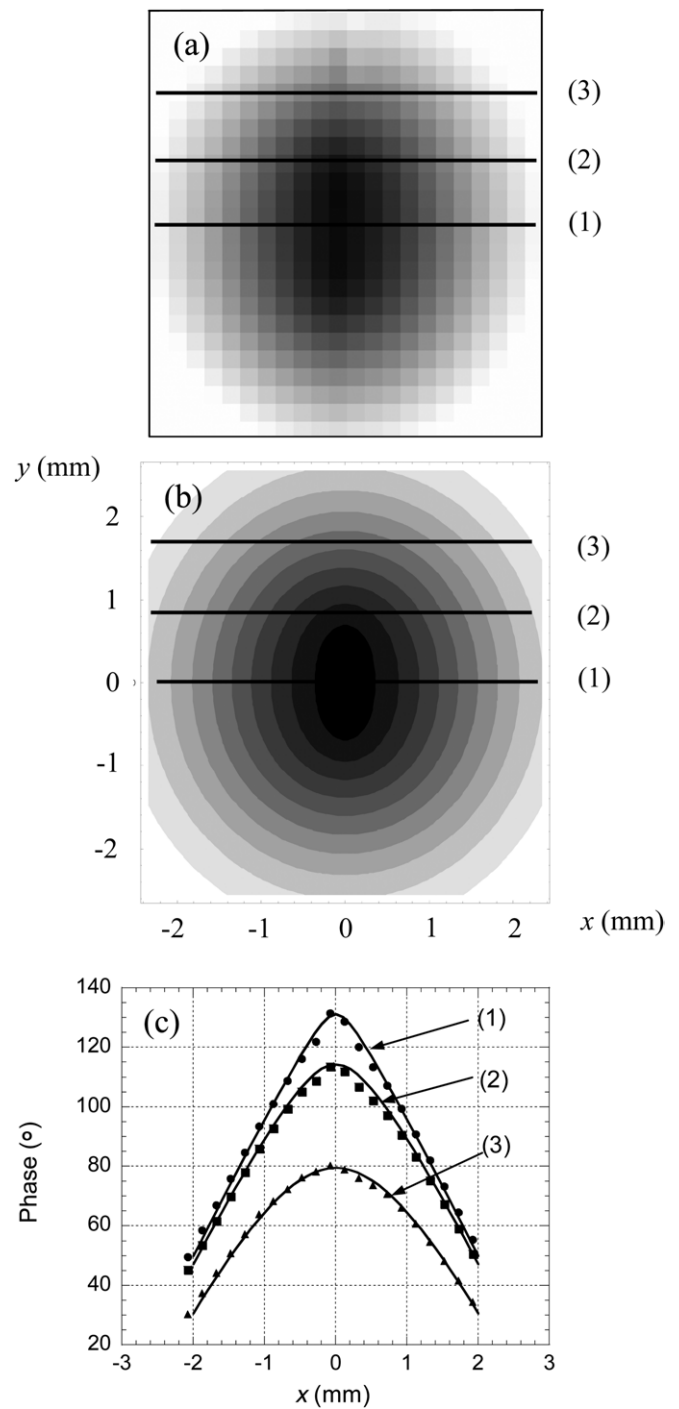


Figure 6. The same as in figure 5 but for the source shown in figure 4(c).

accurately. We believe that these results open a promising way for the estimation of the size and depth of cracks in real specimens from lock-in vibrothermography experiments.

4. Summary and conclusions

In this work we have demonstrated the ability of lock-in vibrothermography to characterize the geometrical parameters and the location of buried heat sources. We have developed a theoretical model to evaluate the surface temperature of

a material containing buried heat sources. The theoretical predictions have been compared with experimental results of lock-in vibrothermography measurements performed with calibrated samples simulating rectangular and uniform heat sources perpendicular to the surface. The agreement between the experimental results and the predictions of the theory opens a promising way to the application of lock-in vibrothermography to the characterization of cracks, in which heat sources are excited at the location of the defects.

Acknowledgments

This work has been supported by the Ministerio de Educación y Ciencia (MAT2005-02999) and by The University of the Basque Country (DIPE06/06).

References

- [1] Carlomagno G M and Berardi P G 1976 *Proc. 3rd Biannual Information Exchange (St Louis)* p 33
- [2] Henneke II E G, Reifsnider K L and Stinchcomb W W 1979 *J. Met.* **31** 11
- [3] Reifsnider K L, Henneke II E G and Stinchcomb W W 1980 *Mechanics of Nondestructive Testing* (New York: Plenum) p 249
- [4] Rantala J, Wu D and Busse G 1996 *Res. Nondestruct. Eval.* **7** 215
- [5] Favro L D, Han X, Ouyang Z, Sun G, Sua H and Thomas R L 2000 *Rev. Sci. Instrum.* **71** 2418
- [6] Favro L D, Han X, Ouyang Z, Sun G and Thomas R L 2001 *Anal. Sci.* **17** s451
- [7] Kremer K-J, Kaiser W and Möller P 1985 *Stahl Eisen* **105** 71
- [8] Rantala J 1993 *Acta Polytech. Scand.—Appl. Phys. Ser.* **186** 1
- [9] Guitonny J, Bozoki Z, Mansanares Am, Leliboux M, Fournier D and Boccara A C 1993 *Opt. Commun.* **104** 61
- [10] Lesniak J R and Boyce B R 1993 *SPIE Proc.* **2001** 92
- [11] Hermosilla Lara s, Joubert P Y, Placko D, Lepoutre F and Piriou M 2002 *QIRT Open Archives* **2** 41
- [12] Bonard J L, Egée M, Menu C, Besnard R, Le Blanc A, Pigeon M and Sellier J Y 1994 *J. Physique. IV* **4** C7-591
- [13] Piau J P, Bendada A, Maldague X and Legoux J-G 2008 *Nondestruct. Testing Eval.* **23** 109
- [14] Dillenz A, Busse G and Wu D 1999 *Proc. SPIE* **3827** 10
- [15] Ouyang Z, Favro L D, Thomas R L and Han X 2002 *Rev. Quant. Nondestruct. Eval.* **21** 577
- [16] Han X, Islam M S, Newaz G, Favro L D and Thomas R L 2005 *J. Appl. Phys.* **98** 014907
- [17] Morbidini M, Cawley P, Barden T, Almond D and Duffour P 2006 *J. Appl. Phys.* **100** 104905
- [18] Krohn N, Stoessel R and Busse G 2002 *Ultrasonics* **40** 633
- [19] Bovsunovsky A P 2004 *Eng. Fract. Mech.* **71** 2271
- [20] Han X, Islam M S, Newaz G, Favro L D and Thomas R L 2006 *J. Appl. Phys.* **99** 074905
- [21] Carslaw H S and Jaeger J C 1959 *Conduction of Heat In Solids* (Oxford: Oxford University Press) 263pp
- [22] Morse P M and Feshbach H 1953 *Methods of Theoretical Physics* (New York: McGraw-Hill) pp 812–6
- [23] Gleiter A, Spiessberger C and Busse G 2007 *QIRT J.* **4** 155
- [24] Lu J, Han X, Newaz G, Favro L D and Thomas R L 2007 *Nondestruct. Eval. Testing* **22** 127